Supporting Information

Enhanced charge transport for wide-bandgap perovskite solar cells enabled by crown ether-mediated crystal modulation

Han Zhong[1], Xuanling Liu[1], Xuanyu Wang[1], Jianfei Yang[1], Ziling Zhang[1], Jinxian Li[1], Jianbo Liu[3], Heping Shen[2,*], and Hong Lin[1,*]

[1]State Key Laboratory of New Ceramics & Fine Processing, School of Materials Science and Engineering, Tsinghua University, Beijing, China.

[2]School of Engineering, The Australian National University, Canberra, ACT, Australia.

[3]Key Laboratory of Advanced Materials of Ministry of Education of China, School of Materials Science and Engineering, Tsinghua University, Beijing, China.

[*]Corresponding author: hong-lin@tsinghua.edu.cn; heping.shen@anu.edu.au.

1. Materials

Lead iodide (PbI_2, 99.99%) was purchased from TCI. Formamidinium iodide (FAI, 98%) was purchased from Greatcell Solar. Cesium iodide (CsI, 99.999%), lead bromide ($PbBr_2$, 99.999%), lead chloride ($PbCl_2$, 99.999%), N,N-dimethylformamide (DMF, anhydrous, 99.8%), dimethyl sulfoxide (DMSO, anhydrous, 99.9%), 2-Propanol (IPA, anhydrous, 99.5%), chlorobenzene (CB, anhydrous, 99.8%), and 4-tert-butyl pyridine (tBP, 98%) were supplied by Sigma-Aldrich. Tin(IV) oxide nanoparticles (12 wt% dispersed in deionized water), methylamine chloride (MACl, 99.5%), phenethylammonium bromide (PEABr, 99.5%), and lithium bis(trifluoromethanesulphonyl)imide (Li-TFSI, 99%) were purchased from Xi'an Polymer Light Technology Co., Ltd. Benzo-18-crown-6-ether (B18C6, 96%) was purchased from Bide Pharmatech Ltd. 2,2',7,7'-Tetrakis[N,N-di(4-methoxyphenyl)amino]-9,9'-spirobifluorene (spiro-OMeTAD, 99.5%) was purchased from Lumtech. Acetonitrile (ACN, 99.9%) was purchased from J&K Scientific. All the chemical reagents were used as received without further purification.

2. Device fabrication

The ITO glasses (15 Ω/sq, Advanced Election Technology Co., Ltd.) were cleaned in a sequence of detergent, deionized water, ACN, and IPA with 15 min ultra-sonication for each step. Before the deposition of SnO_2 layer, the substrates were treated with oxygen plasma for 15 min. Tin(IV) oxide nanoparticles (diluted into 2.5 wt% with deionized water) was spin-coated at 4000 rpm for 30 s, and then annealed at 150 °C for 30 min. Before the deposition of perovskite layer, the samples were treated with oxygen plasma for 2 min, and then transferred into a N_2 glovebox. The perovskite precursor solution was prepared by dissolving 4.7 mg MACl, 11.7 mg $PbCl_2$, 80.0 mg CsI, 115.6

mg $PbBr_2$, 187.8 mg FAI, and 500.2 mg PbI_2 in 1 mL DMF/DMSO mixture with a volume ratio of 3:1. For the deposition of perovskite layer, the precursor solution was spin-coated at 5000 rpm for 20 s. 100 μL CB was quickly dropped onto the center of the sample 5 s before the end of the process as anti-solvent. For the target group, 0.005 mg/ml B18C6 was added in CB. The samples were then annealed at 100 °C for 30 min. After that, PEABr (2 mg/ml in IPA) was spin-coated at 6000 rpm for 60 s. 72.3 mg spiro-OMeTAD powder was dissolved in 1 mL CB, with the addition of 29 μL tBP and 35 μL Li-TFSI (260 mg/mL in ACN). The spiro-OMeTAD solution was then spin-coated at 4000 rpm for 30 s. The samples were kept in a dry box (<10 RH%) overnight for oxidation. Finally, 70 nm Au was deposited by thermal evaporation under a vacuum of 1×10^{-4} Pa.

3. Characterization

The ultraviolet-visible transmission spectrum was obtained using a UV-Vis spectrophotometer (Lambda 1050, PerkinElmer, USA) at room temperature.

The surface morphology of perovskite films and cross section of PSCs were observed with the field-emission scanning electron microscope (SEM, LEO1530, Zeiss, Germany).

The crystal structures of thin films were obtained by an X-ray diffractometer (D8 Advance, Bruker, German) with Cu Kα (λ=1.5406 Å) radiation at 40 kV.

The photocurrent density-voltage (*J-V*) characteristics of PSCs were measured with a digital source meter (2400, Keithley Instruments, USA) under AM 1.5G illumination (100 mW/cm^2) by a solar simulator (91192, Oriel, USA) calibrated with a standard crystalline silicon solar cell. The active area of PSCs was 0.06 cm^2.

The monochromatic incident photon-to-electron conversion efficiency (IPCE) were measured by a solar cell quantum efficiency measurement system (QEX10, PV measurements, USA). The intensity of incident monochromatic light was calibrated with a standard silicon solar cell (1H020, PV Measurements, USA) in DC mode.

Electrochemical impedance spectroscopy (EIS) and capacitance-voltage (*C-V*) were measured using a Zahner system (Zahner, Zahner-Electric GmbH & Co., KG, Germany). EIS was recorded at a bias of 1.0 V with a modulation amplitude of 10 mV at frequencies ranging from 1 Hz to 1 MHz in the dark.

For Mott-Schottky Plot, an AC signal with an amplitude of 20 mV and a frequency of 10 kHz was adopted.

X-ray photoelectron spectra (XPS) were recorded by photoelectron spectrometer (ESCALAB 250Xi, Thermo Fisher Scientific Inc., USA) with Al Kα radiation (hν = 1486.6 eV) to analyze the element information. The photoelectron spectroscopy in the air (PESA) was performed with the AC-2 PESA instrument (AC-2, RKI INSTRUMENTS, Japan) combining an open counter with a UV source to position the valence band. The surface morphology and conductivity of perovskite films was measured by atomic force microscopy (AFM, Cypher, Oxford Instruments, UK).

Fourier transform infrared spectroscopy (FTIR) measurements were performed using the ATR (Attenuated Total Reflection) mode on the infrared spectrometer (VERTEX 70V, Bruker, Germany).

The photoluminescence (PL) spectra were characterized by a fluorescence spectrometry (FLS920,

Edinburgh Instruments, UK). Steady-state PL measurements were carried out by exciting the sample with a monochromatic xenon lamp source with a central wavelength of 450 nm. Time-resolved PL (TRPL) measurements were performed via a time-correlated single-photon counting system using a pulsed laser beam (EPL405) with a wavelength of 405 nm.

4. Calculation

First-principles density functional theory (DFT) calculations were performed using the Vienna Ab initio Simulation Package (VASP) [1] with the projector augmented wave (PAW) method [2]. The exchange-functional was treated within the generalized gradient approximation (GGA) employing the Perdew-Burke-Ernzerhof (PBE) functional [3]. The long-range van der Waals interactions are accounted for through the DFT-D3 approach [4]. A plane wave basis set with an energy cutoff of 500 eV was employed, and the geometry relaxation was performed until the forces on each atom were below 0.03 eV/Å. The Brillouin zone was sampled using 1 × 1 × 1 k-point grid. Self-consistent calculations were conducted with an energy convergence threshold of 10^{-5} eV. To prevent interactions between periodic structures, a vacuum region of 15 Å was added along the z direction.

The adsorption energy of the PMS is obtained by the following formula:

$E_{ads} = E_{*mol} - E_{*} - E_{mol}$

Where, E_{*mol} represents the total energy of molecule adsorbed on the slab, E_{*} represents the total energy of the slab, and E_{mol} represents the energy of molecule.

[1] G. Kresse, J. Furthmüller, Efficiency of ab-initio total energy calculations for metals and semiconductors using a plane-wave basis set, Comp. Mater. Sci. 6 (1996) 15–50.

[2] P.E. Blo ̈chl, O. Jepsen, O.K. Andersen, Improved tetrahedron method for brillouin- zone integrations, Phys. Rev. B Condens. Matter 49 (1994) 16223–16233.

[3] J.P. Perdew, J.A. Chevary, S.H. Vosko, K.A. Jackson, M.R. Pederson, D.J. Singh, C. Fiolhais, Erratum: atoms, molecules, solids, and surfaces: applications of the generalized gradient approximation for exchange and correlation, Phys. Rev. B Condens. Matter 48 (1993), 4978-4978.

[4] Grimme S, Antony J, Ehrlich S and Krieg H 2010 A consistent and accurate ab initio parametrization of density functional dispersion correction (DFT-D) for the 94 elements H-Pu Journal of Chemical Physics 2010, 132, 154104.

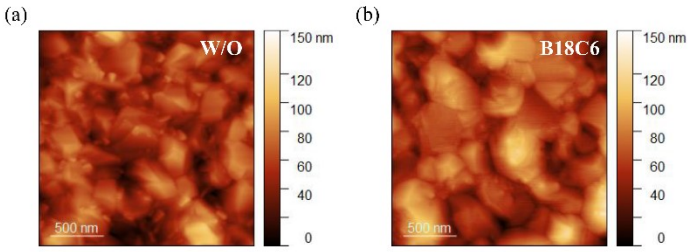

Figure S1 AFM images of perovskite films (a) without and (b) with B18C6 modification.

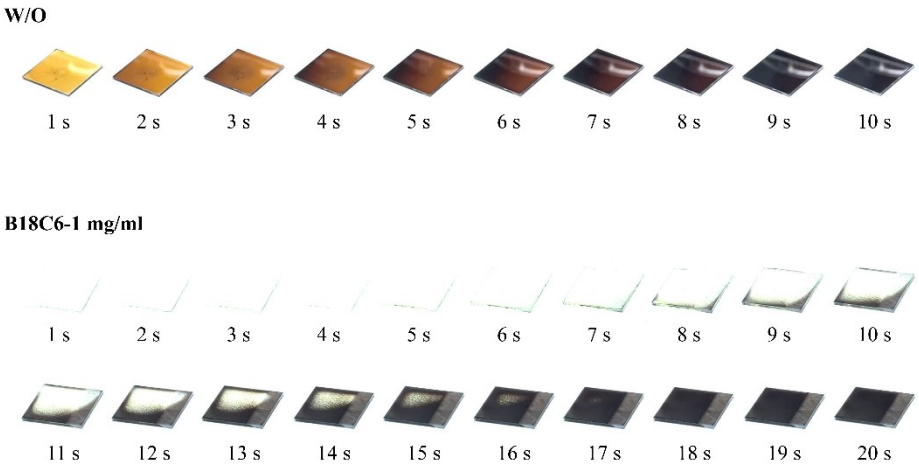

Figure S2 Photographs of perovskite films annealed with different durations. Note that the film morphology has changed due to the high concentration of B18C6 for clear observation.

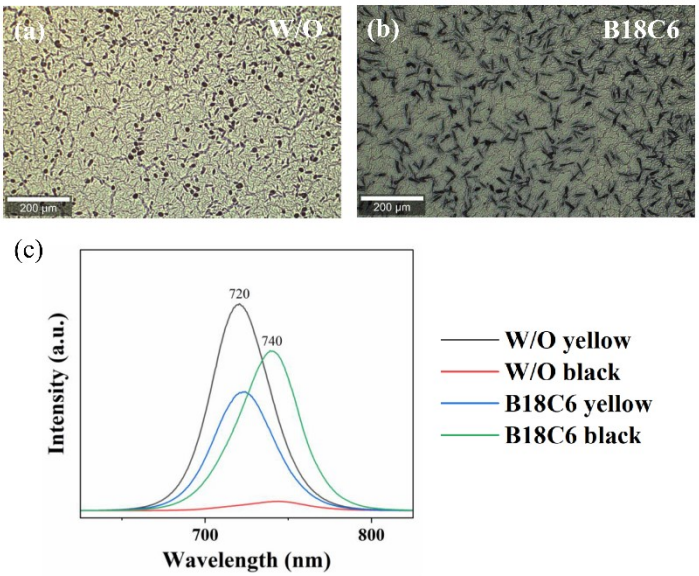

Figure S3 Optical microscopy images of wet-films (a) without and (b) with B18C6 modification. (c) PL of different regions in the wet-films.

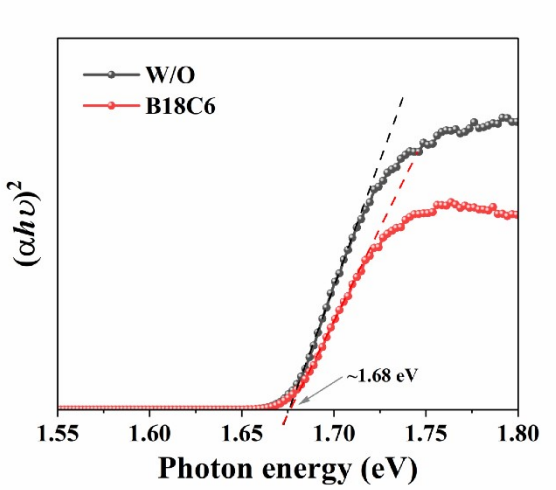

Figure S4 Calculating the bandgap of perovskite films by Tauc plot.

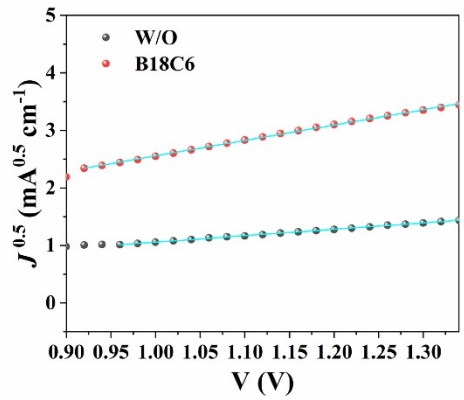

Figure S5 Calculating the mobility of perovskite films by fitting Mott-Gurney equation in the SCLC regime.

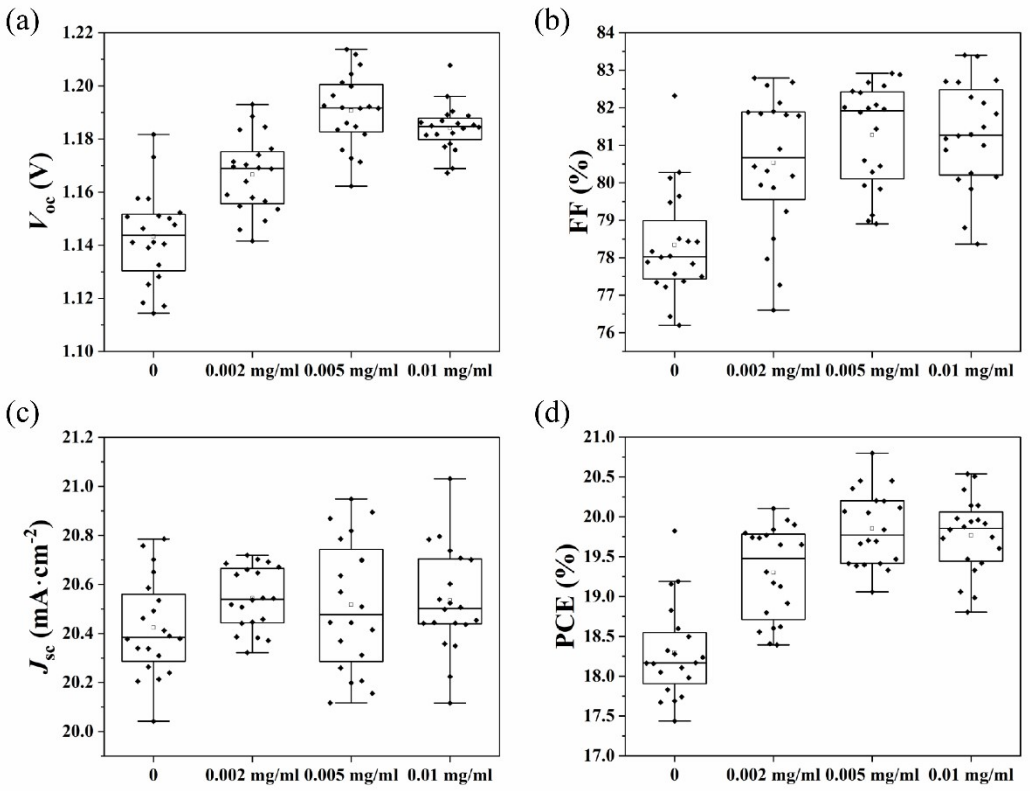

Figure S6 The performance dependence on the B18C6 amount. (a) V_{oc}, (b) FF, (c) J_{sc}, and (d) PCE.

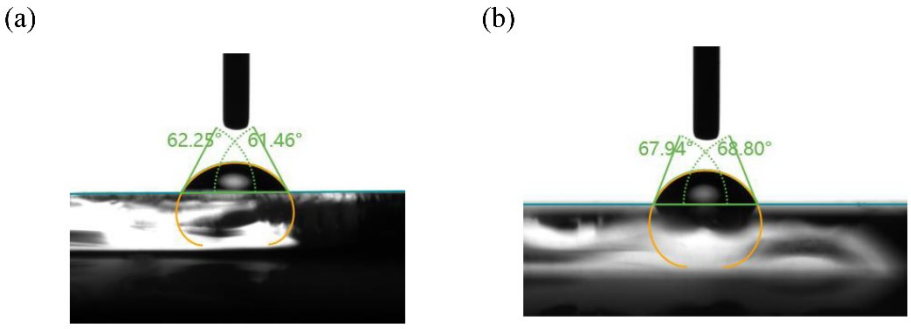

Figure S7 Contact angle of perovskite films (a) without and (b) with B18C6 modification.

Table S1 Fitting results of TRPL

	A_1	τ_1 (ns)	A_2	τ_2 (ns)	τ_{avg} (ns)
W/O on glass	218.742	63.1801	534.778	724.7352	701.9575
B18C6 on glass	943.597	5.8675	654.135	1056.4703	1048.12
W/O on ETL	429.196	22.8993	1213.025	498.3432	490.7369
B18C6 on ETL	393.414	39.2012	1077.56	348.3581	336.1577

The results of TRPL were fitted by $y = A_1 e^{-t/\tau_1} + A_2 e^{-t/\tau_2}$, and the average lifetime was

calculated by $\tau_{avg} = \frac{A_1\tau_1^2 + A_2\tau_2^2}{A_1\tau_1 + A_2\tau_2}$.

Table S2 Statistical photovoltaic parameters of devices

	V_{OC} (V) Mean ± SD	J_{SC} (mA cm^{-2}) Mean ± SD	FF (%) Mean ± SD	PCE (%) Mean ± SD
W/O	1.173 ± 0.011	20.48 ± 0.21	77.93 ± 1.56	18.72 ± 0.51
B18C6	1.190 ± 0.015	20.57 ± 0.22	81.47 ± 1.76	19.94 ± 0.55

Table S3 Statistical photovoltaic parameters of devices

Concentration (mg/mL)	V_{OC} (V) Mean ± SD	J_{SC} (mA cm$^{-2)}$ Mean ± SD	FF (%) Mean ± SD	PCE (%) Mean ± SD
0	1.143 ± 0.018	20.42 ± 0.20	78.34 ± 1.44	18.30 ± 0.59
0.002	1.167 ± 0.014	20.54 ± 0.13	80.53 ± 1.85	19.30 ± 0.58
0.005	1.191 ± 0.014	20.52 ± 0.27	81.27 ± 1.37	19.85 ± 0.47
0.01	1.184 ± 0.009	20.53 ± 0.21	81.28 ± 1.41	19.77 ± 0.48